# Interactions of $B_c$ mesons in relativistic heavy-ion collisions

Shaheen Irfan,[1,2,*] Faisal Akram,[2,†] Bilal Masud,[2,‡] and Bushra Shafaq[2,§]
[1]*Department of Physics, The University of Lahore, UOL, Defence Road Campus, Lahore 54000, Pakistan*
[2]*Center for High Energy Physics, Punjab University, Lahore 54590, Pakistan*

(Received 2 August 2019; published 18 December 2019)

The enhancement of $B_c$ production is expected due to formation of quark-gluon plasma in heavy-ion collisions. However, it is also expected that the production rate of $B_c$ meson can be affected by its interactions with comovers in hot hadronic gas. To study this effect we calculate the dissociation cross sections of $B_c$ meson by $\pi$ and $\rho$ mesons, including anomalous processes using an effective hadronic Lagrangian. Thermal averaged cross sections of $B_c$ are evaluated with a form factor when a cutoff parameter in it is 1 and 2 GeV. Using these cross sections in the kinetic equation, we study the time evolution of $B_c$ mesons in hot hadronic matter formed at LHC. We find that the effect of interactions with comovers is small but not negligible.

DOI: 10.1103/PhysRevC.100.064906

## I. INTRODUCTION

In 1986 Matsui and Satz [1] hypothesized that in a deconfined medium color screening would have dissociated $J/\psi$ mesons, resulting in its suppressed yield. This deconfined state of matter is called quark-gluon plasma (QGP). Thus, suppression of $J/\psi$ could be considered as a probe for QGP. Anomalously large $J/\psi$ suppression was observed by NA50 experiment at CERN [2] with moderate to large transfer energy in Pb+Pb collisions at $P_{\rm Lab} = 158$ GeV/c. However, this observed suppression may also occur due to dissociation by comoving hadrons mainly $\pi$ and $\rho$ mesons, especially if the dissociation cross section is at least a few mb [3–8]. To calculate these cross sections, quark potential models, perturbative QCD [9], QCD sum-rule approach [10,11], and flavor symmetric effective Lagrangian [12–15] have been used. Analogous to charmonium, suppression of bottomonium states was also predicted during QGP phase [1]. Recently it was observed by CMS in Pb+Pb collisions that excited states of bottomonium are strongly suppressed [16]. To have an unambiguous interpretation of the observed signal, the information of the dissociation cross section is also needed [13,17].

It has been suggested that the production rate of heavy mixed flavor hadrons would also be affected in the presence of QGP [18–20]. For $B_c$ meson, which is bound state of $\bar{b}c$ or $b\bar{c}$, it is expected that production rate could be enhanced in the presence of QGP [19,21,22]. QGP contains many unpaired $b(\bar{b})$ and $c(\bar{c})$ quarks due to color Debye screening. These unpaired $b(\bar{b})$ and $c(\bar{c})$ quarks upon encountering each other could form $B_c$ mesons and due to relatively large binding energy, $B_c$ mesons probably survive in QGP [22]. However, the observed production rate may also depend upon the dissociation cross section by the hadronic comovers.

In Ref. [22] $B_c$ dissociation by nucleons is examined using meson-baryon exchange model. The calculated cross sections are in the range of a few millibarn. Recently in Ref. [23], using the same couplings and hadronic Lagrangian within the meson exchange model, the dissociation of $B_c$ meson by $\pi$ meson is studied. The resulting cross sections with form factors are in the range 2–7 mb and 0.2–2 mb for the processes $B_c^+ + \pi \to D + B$ and $B_c^+ + \pi \to D^* + B^*$, respectively. The form factors are included to incorporate the effect finite size of hadrons. In Ref. [24], the dissociation of $B_c$ meson by $\rho$ mesons is studied. The calculated cross sections of the processes $B_c^+ + \rho \to D^* + B$ and $B_c^+ + \rho \to D + B^*$ with form factor are found in the range of 0.6–3 and 0.05–0.3 mb, respectively. In this paper, we investigate the $B_c$ dissociation by $\pi$ and $\rho$ mesons including anomalous couplings like PVV (pseudo-vector-vector), PPPV, and PVVV, which are ignored in the previous studies. The inclusion of these couplings results in the opening of new dissociation channels and the addition of new processes and extra diagrams. The contribution of anomalous couplings is found to be significant for calculating the cross sections of charmonium dissociation with $\pi$ and $\rho$ meson in Ref. [25], $K$ mesons in Ref. [26], and dissociation of $B_c$ meson by nucleons in Ref. [27]. We also calculate the thermal averaged cross sections and study the time evolution of $B_c$ meson in hot hadron gas at LHC using a schematic expanding fireball model with an initial $B_c$ abundance determined by perturbative QCD (pQCD) assuming that all heavy flavor pairs are produced at the initial stage through hard parton collisions.

The paper is organized as follows. In Sec. II, the interaction Lagrangian terms that are relevant for the description of the dissociation of $B_c$ by $\pi$ and $\rho$ mesons, including anomalous processes, are given. The analytical expressions of the amplitudes of dissociation cross sections are also reported

*shaheen.irfan@phys.uol.edu.pk
†faisal.chep@pu.edu.pk
‡bilalmasud.chep@pu.edu.pk
§bshafaq.chep@pu.edu.pk

 

in this section. In Sec. III, we calculate the cross sections with and without form factor and their thermal averaged values. In Sec. IV, we study the time evolution of the $B_c$ meson abundance at LHC in a schematic model followed by concluding remarks in Sec. V.

## II. INTERACTION LAGRANGIAN AND AMPLITUDES OF $B_c$ MESON DISSOCIATION

### A. Interaction Lagrangian

We consider the following reactions using an effective Hadronic Lagrangian:

$$\begin{aligned}
&B_c^+ + \pi \to D + B, \quad B_c^- + \pi \to \bar{D} + \bar{B} \quad B_c^+ + \rho \to D + B, \quad B_c^- + \rho \to \bar{D} + \bar{B},\\
&B_c^+ + \pi \to D^* + B, \quad B_c^- + \pi \to \bar{D}^* + \bar{B}, \quad B_c^+ + \rho \to D^* + B, \quad B_c^- + \rho \to \bar{D}^* + \bar{B},\\
&B_c^+ + \pi \to D + B^*, \quad B_c^- + \pi \to \bar{D} + \bar{B}^*, \quad B_c^+ + \rho \to D + B^*, \quad B_c^- + \rho \to \bar{D} + \bar{B}^*,\\
&B_c^+ + \pi \to D^* + B^*, \quad B_c^- + \pi \to \bar{D}^* + \bar{B}^*, \quad B_c^+ + \rho \to D^* + B^*, \quad B_c^- + \rho \to \bar{D}^* + \bar{B}^*.
\end{aligned} \tag{1}$$

In each row the processes of the first two entries are charge conjugates, as are the last two entries. These charge conjugate processes have the same cross sections. Each process in Eq. (1) is a generic form of the processes given by different charged states of $\pi$, $\rho$, $D$, $D^*$, $B$, and $B^*$ mesons. For example, the process $B_c^+ + \pi \to D + B$ represents the following processes:

$$B_c^+ + \pi^+ \to D^+ + B^+, \quad B_c^+ + \pi^- \to D^0 + B^0, \quad B_c^+ + \pi^0 \to D^+ + B^0 \quad B_c^+ + \pi^0 \to D^0 + B^+. \tag{2}$$

For calculating the cross sections of the above reactions, relevant interaction Lagrangian terms are required. The required terms for normal processes (for which the relevant couplings are dimensionless) are obtained using the method described in Refs. [23,24] and are given as follows.

**PPV Couplings:**

$$\mathcal{L}_{\pi DD^*} = ig_{\pi DD^*}\, D^{*\mu}\vec{\tau}\cdot(\bar{D}\partial_\mu\vec{\pi} - \partial_\mu\bar{D}\vec{\pi}) + \text{Hc}, \tag{3a}$$

$$\mathcal{L}_{\pi BB^*} = ig_{\pi BB^*}\, \bar{B}^{*\mu}\vec{\tau}\cdot(B\partial_\mu\vec{\pi} - \partial_\mu B\vec{\pi}) + \text{Hc}, \tag{3b}$$

$$\mathcal{L}_{B_cBD^*} = ig_{B_cBD^*}\, \bar{D}^{*\mu}\,(B_c^-\partial_\mu\bar{B} - \partial_\mu B_c^-\bar{B}) + \text{Hc}, \tag{3c}$$

$$\mathcal{L}_{B_cB^*D} = ig_{B_cB^*D}\, B^{*\mu}\,(B_c^-\partial_\mu D - \partial_\mu B_c^- D) + \text{Hc}, \tag{3d}$$

$$\mathcal{L}_{\rho DD} = ig_{\rho DD}(D\vec{\tau}\partial_\mu\bar{D} - \partial_\mu D\vec{\tau}\bar{D})\cdot\vec{\rho}^{\,\mu}, \tag{3e}$$

$$\mathcal{L}_{\rho BB} = ig_{\rho BB}\;\vec{\rho}^{\,\mu}\cdot(\bar{B}\vec{\tau}\partial_\mu B - \partial_\mu\bar{B}\vec{\tau}B). \tag{3f}$$

**VVV Couplings:**

$$\begin{aligned}
\mathcal{L}_{\rho D^*D^*} = {}& ig_{\rho D^*D^*}[\vec{\rho}^{\,\mu}\cdot(\partial_\mu D^{*\nu}\vec{\tau}\bar{D}^*_\nu - D^{*\nu}\vec{\tau}\partial_\mu\bar{D}^*_\nu)\\
&+ \bar{D}^{*\mu}\cdot(D^{*\nu}\vec{\tau}\cdot\partial_\mu\vec{\tau}_\nu - \partial_\mu D^{*\nu}\vec{\tau}\cdot\vec{\rho}_\nu)\\
&+ D^{*\mu}\cdot(\vec{\tau}\cdot\vec{\tau}^{\,\nu}\partial_\mu\bar{D}^*_\nu - \vec{\tau}\cdot\partial_\mu\vec{\rho}^{\,\nu}\bar{D}^*_\nu)],
\end{aligned} \tag{4a}$$

$$\begin{aligned}
\mathcal{L}_{\rho B^*B^*} = {}& ig_{\rho B^*B^*}[\vec{\rho}^{\,\mu}\cdot(\partial_\mu\bar{B}^{*\nu}\vec{\tau}B^*_\nu - \bar{B}^{*\nu}\vec{\tau}\partial_\mu B^*_\nu)\\
&+ B^{*\mu}\cdot(\bar{B}^{*\nu}\vec{\tau}\cdot\partial_\mu\vec{\rho}_\nu - \partial_\mu\bar{B}^{*\nu}\vec{\tau}\cdot\vec{\rho}_\nu)\\
&+ \bar{B}^{*\mu}\cdot(\vec{\tau}\cdot\vec{\rho}^{\,\nu}\partial_\mu B^*_\nu - \vec{\tau}\cdot\partial_\mu\vec{\rho}^{\,\nu}B^*_\nu)].
\end{aligned} \tag{4b}$$

**PPVV Couplings:**

$$\mathcal{L}_{\pi B_cD^*B^*} = -g_{\pi B_cD^*B^*}B_c^+\bar{B}^{*\mu}\vec{\tau}\cdot\vec{\pi}\bar{D}^*_\mu + \text{Hc}, \tag{5a}$$

$$\mathcal{L}_{\rho B_cD^*B} = g_{\rho B_cD^*B}\, B_c^+\bar{B}\vec{\tau}\cdot\vec{\rho}_\mu\bar{D}^{*\mu} + \text{Hc}, \tag{5b}$$

$$\mathcal{L}_{\rho B_cDB^*} = g_{\rho B_cDB^*}\, B_c^+\bar{B}^{*\mu}\vec{\tau}\cdot\vec{\rho}_\mu\bar{D} + \text{Hc}. \tag{5c}$$

Where "Hc" represents the Hermitian conjugate of the corresponding term. In addition to the above normal terms, there are anomalous terms as well, which are required to give a complete description of the hadronic processes. The required interaction Lagrangian terms for the anomalous processes (for which the relevant couplings are not dimensionless) are obtained using the method described in Ref. [25] and are given as follows.

**PVV Couplings:**

$$\mathcal{L}_{\pi D^*D^*} = -g_{\pi D^*D^*}\varepsilon^{\mu\nu\alpha\beta}[(\partial_\mu D^*_\nu)\vec{\tau}\cdot\vec{\pi}(\partial_\alpha\bar{D}^*_\beta)], \tag{6a}$$

$$\mathcal{L}_{\pi B^*B^*} = g_{\pi B^*B^*}\varepsilon^{\mu\nu\alpha\beta}[\left(\partial_\alpha\bar{B}^*_\beta\right)\vec{\tau}\cdot\vec{\pi}(\partial_\mu B^{*\nu})], \tag{6b}$$

$$\begin{aligned}
\mathcal{L}_{B_cD^*B^*} = {}& g_{B_cD^*B^*}\varepsilon^{\mu\nu\alpha\beta}[(\partial_\mu D^*_\nu)(\partial_\alpha B^{*\beta})B_c{}^-\\
&+ B_c{}^+(\partial_\alpha\bar{B}^{*\beta})(\partial_\mu\bar{D}^{*\nu})],
\end{aligned} \tag{6c}$$

$$\mathcal{L}_{\rho D^*D} = -g_{\rho D^*D}\varepsilon^{\mu\nu\alpha\beta}(D\partial_\mu\rho_\nu\partial_\alpha\bar{D}^*_\beta + \partial_\mu D^*_\nu\partial_\alpha\rho_\beta\bar{D}), \tag{6d}$$

$$\mathcal{L}_{\rho B^*B} = -g_{\rho B^*B}\;\varepsilon^{\mu\nu\alpha\beta}(B\partial_\mu\rho_\nu\partial_\alpha\bar{B}^*_\beta + \partial_\mu B^*_\nu\partial_\alpha\rho_\beta\bar{B}). \tag{6e}$$

**PPPV Couplings:**

$$\begin{aligned}
\mathcal{L}_{\pi B_cD^*B} = {}& -ig_{\pi B_cD^*B}\varepsilon^{\mu\nu\alpha\beta}[D^*_\mu(\partial_\nu B_c^-)(\vec{\tau}\cdot\partial_\alpha\vec{\pi})(\partial_\beta B)\\
&+ \bar{D}^*_\mu(\vec{\tau}\cdot\partial_\nu\vec{\pi})(\partial_\alpha B_c^+)(\partial_\beta\bar{B})],
\end{aligned} \tag{7a}$$

$$\begin{aligned}
\mathcal{L}_{\pi B_cDB^*} = {}& -ig_{\pi B_cDB^*}\varepsilon^{\mu\nu\alpha\beta}[B^*_\mu(\partial_\nu B_c^-)(\vec{\tau}\cdot\partial_\alpha\vec{\pi})(\partial_\beta D)\\
&+ \bar{B}^*_\mu(\partial_\nu B_c^+)(\vec{\tau}\cdot\partial_\alpha\vec{\pi})(\partial_\beta\bar{D})],
\end{aligned} \tag{7b}$$

$$\begin{aligned}
\mathcal{L}_{\rho B_cBD} = {}& -ig_{\rho B_cBD}\varepsilon^{\mu\nu\alpha\beta}[\rho_\mu(\partial_\nu D)(\partial_\alpha B)(\partial_\beta B_c^-)\\
&+ \rho_\mu(\partial_\nu\overline{B})(\partial_\alpha\bar{D})(\partial_\beta B_c^+)].
\end{aligned} \tag{7c}$$

**PVVV Couplings:**

$$\begin{aligned}
&\mathcal{L}_{\rho B_cB^*D^*}\\
&= ig_{\rho B_cD^*B^*}\varepsilon^{\mu\nu\alpha\beta}[B^*_\mu\rho_\nu D^*_\alpha(\partial_\beta B_c^-) + \bar{D}^*_\mu\rho_\nu\bar{B}^*_\alpha(\partial_\beta B_c^+)]\\
&\quad - ih_{\rho B_cD^*B^*}\left[B_c^-(\partial_\mu D^*_\nu)\vec{\tau}\cdot\vec{\rho}_\alpha B^*_\beta + B_c^+(\partial_\mu\bar{B}^*_\nu)\rho_\alpha\bar{D}^*_\beta\right].
\end{aligned} \tag{8a}$$

In Eqs. (3)–(8) $\vec{\tau}$ represents Pauli spin matrices, and $\vec{\pi}$ and $\vec{\rho}$ represent isospin triplets:

$$\vec{\pi} = (\pi_1, \pi_2, \pi_3), \quad \vec{\rho} = (\rho_1, \rho_2, \rho_3).$$

Also, $\pi^{\pm} = \frac{1}{\sqrt{2}}(\pi_1 \mp \pi_2)$, $\pi^0 = \pi_3$, and likewise $\rho^{\pm}$ and $\rho^0$ are defined. The vector and pseudoscalar charm and bottom meson doublets are given as

$$\bar{D}^*_\mu = \left(\bar{D}^{*0}_\mu, D^{*-}_\mu\right)^T,\ \bar{D} = (\bar{D}^0, D^-)^T,\ D = (D^0, D^+),$$

$$B^*_\mu = \left(B^{*+}_\mu, B^{*0}_\mu\right)^T,\quad \bar{B} = (B^-, \bar{B}^0),\quad B = (B^+, B^0)^T.$$

In Eq. (1), for the case of $\pi$; there is no anomalous contribution to the process $B_c^+ + \pi \to D + B$, the processes $B_c^+ + \pi \to D^* + B$ and $B_c^+ + \pi \to D + B^*$ appear after including the anomalous couplings, and two additional diagrams are added in the process $B_c^+ + \pi \to D^* + B^*$. For the case of $\rho$; $B_c^+ + \rho \to D + B$ and $B_c^+ + \rho \to D^* + B^*$ are the new processes appearing after including the anomalous couplings and in case of processes $B_c^+ + \rho \to D^* + B$ and $B_c^+ + \rho \to D + B^*$, anomalous couplings contribute one additional diagram, respectively.

### B. Amplitudes of dissociation cross sections

For calculating the cross sections of $B_c$ dissociation by $\pi$ and $\rho$ mesons, we use the effective Lagrangian given in Eqs. (3)–(8). In this paper, we are only reporting the scattering amplitudes of the anomalous processes and of additional diagrams that are dependent on the anomalous couplings. Dissociation amplitudes of other diagrams that depend only on normal couplings are given in Refs. [23,24]. Diagrams of the process $B_c^+ + \pi \to D^* + B$ are shown in Fig. 1 (2a to 2c) and corresponding amplitudes are

$$M_{2a} = g_{\pi D^* D^*} g_{B_c B D^*}\ \varepsilon_{\mu\nu\alpha\sigma} p_3^\mu (p_3 - p_1)_\beta \frac{-i}{t - m_{D^*}^2}\left(g^{\alpha\sigma} - \frac{(p_1 - p_3)^\alpha (p_1 - p_3)^\sigma}{m_{D^*}^2}\right)(-p_2 - p_4)^\nu \varepsilon_{D^*}^\beta(p_3), \tag{9a}$$

$$M_{2b} = g_{\pi B B^*} g_{B_c B^* D^*}\ \varepsilon_{\mu\nu\alpha\sigma} p_3^\mu (p_1 + p_4)^\nu \frac{-i}{u - m_{B^*}^2}\left(g^{\alpha\sigma} - \frac{(p_1 - p_4)^\alpha (p_1 - p_4)^\sigma}{m_{B^*}^2}\right)(p_3 - p_2)_\beta \varepsilon_{D^*}^\beta(p_3), \tag{9b}$$

$$M_{2c} = -i g_{\pi B_c B D^*}\ \varepsilon_{\mu\nu\alpha\beta} p_1^\alpha p_4^\mu p_2^\nu \varepsilon_{D^*}^\beta(p_3), \tag{9c}$$

and the full amplitude is written as

$$M_2 = M_{2a} + M_{2b} + M_{2c}. \tag{9d}$$

Diagrams of the process $B_c^+ + \pi \to D + B^*$ are shown in Fig. 1 (3a to 3c) and corresponding amplitudes are

$$M_{3a} = g_{\pi D^* D} g_{B_c B^* D^*}\ \varepsilon_{\mu\nu\alpha\sigma} p_4^\mu (p_4 - p_2)_\beta \frac{-i}{t - m_{D^*}^2}\left(g^{\alpha\sigma} - \frac{(p_1 - p_3)^\alpha (p_1 - p_3)^\sigma}{m_{D^*}^2}\right)(p_1 + p_3)^\nu \varepsilon_{B^*}^\beta(p_4), \tag{10a}$$

$$M_{3b} = g_{\pi B^* B^*} g_{B_c B^* D}\ \varepsilon_{\mu\nu\alpha\sigma} p_4^\mu (p_4 - p_1)_\beta \frac{-i}{u - m_{B^*}^2}\left(g^{\alpha\sigma} - \frac{(p_1 - p_4)^\alpha (p_1 - p_4)^\sigma}{m_{D^*}^2}\right)(-p_2 - p_3)^\nu \varepsilon_{B^*}^\beta(p_4), \tag{10b}$$

$$M_{3c} = -i g_{\pi B_c D B^*}\ \varepsilon_{\mu\nu\alpha\beta} p_2^\alpha p_3^\mu p_1^\nu \varepsilon_{B^*}^\beta(p_4), \tag{10c}$$

and the full amplitude is written as

$$M_3 = M_{3a} + M_{3b} + M_{3c}. \tag{10d}$$

Diagrams of the process $B_c^+ + \pi \to D^* + B^*$ are shown in Fig. 1 (4a to 4e). The amplitudes of diagram 4d and 4e which depend on anomalous couplings are

$$M_{4d} = g_{\pi D^* D^*} g_{B_c B^* D^*} \varepsilon_{\sigma\lambda\alpha\beta} \varepsilon^{\sigma\lambda}_{\gamma\zeta} p_4^\gamma (p_3 - p_1)_\mu \frac{-i}{t - m_{D^*}^2}\left(g^{\alpha\beta} - \frac{(p_1 - p_3)^\alpha (p_1 - p_3)^\beta}{m_{D^*}^2}\right) p_3^\zeta (p_4 - p_2)_\nu \varepsilon_{D^*}^\mu(p_3) \varepsilon_{B^*}^\nu(p_4), \tag{11a}$$

$$M_{4e} = g_{\pi B^* B^*} g_{B_c D^* B^*} \varepsilon_{\sigma\lambda\alpha\beta} \varepsilon^{\sigma\lambda}_{\gamma\zeta} (p_4 - p_1)_\nu p_3^\gamma \frac{-i}{u - m_{B^*}^2}\left(g^{\alpha\beta} - \frac{(p_1 - p_4)^\alpha (p_1 - p_4)^\beta}{m_{B^*}^2}\right)(p_3 - p_2)_\mu p_4^\zeta \varepsilon_{D^*}^\mu(p_3) \varepsilon_{B^*}^\nu(p_4), \tag{11b}$$

and the full amplitude is written as

$$M_4 = M_{4a} + M_{4b} + M_{4c} + M_{4d} + M_{4e}. \tag{11c}$$

Now we report the amplitudes of the anomalous diagrams of $B_c$ dissociation by $\rho$. Diagrams of the process $B_c^+ + \rho \to D + B$ are shown in Fig. 2 (5a to 5c) and corresponding amplitudes are

$$M_{5a} = g_{B_c B D^*} g_{\rho D^* D} \varepsilon_{\sigma\nu\alpha\beta} p_1^\nu (-p_2 - p_4)^\sigma \frac{-i}{t - m_{D^*}^2}\left(g^{\alpha\beta} - \frac{(p_1 - p_3)^\alpha (p_1 - p_3)^\beta}{m_{D^*}^2}\right)(p_3 - p_1)_\mu \varepsilon_\rho^\mu(p_1), \tag{12a}$$

$$M_{5b} = g_{\rho B^* B} g_{B_c B^* D} \varepsilon_{\sigma\nu\alpha\beta} p_1^\sigma \frac{-i}{u - m_{B^*}^2}(-p_3 - p_2)^\nu \left(g^{\alpha\beta} - \frac{(p_1 - p_4)^\alpha (p_1 - p_4)^\beta}{m_{B^*}^2}\right)(p_4 - p_1)_\mu \varepsilon_\rho^\mu(p_1), \tag{12b}$$

$$M_{5c} = -i g_{\rho B_c B D} \varepsilon_{\mu\nu\alpha\beta} p_2^\nu p_3^\alpha p_4^\beta \varepsilon_\rho^\mu(p_1), \tag{12c}$$

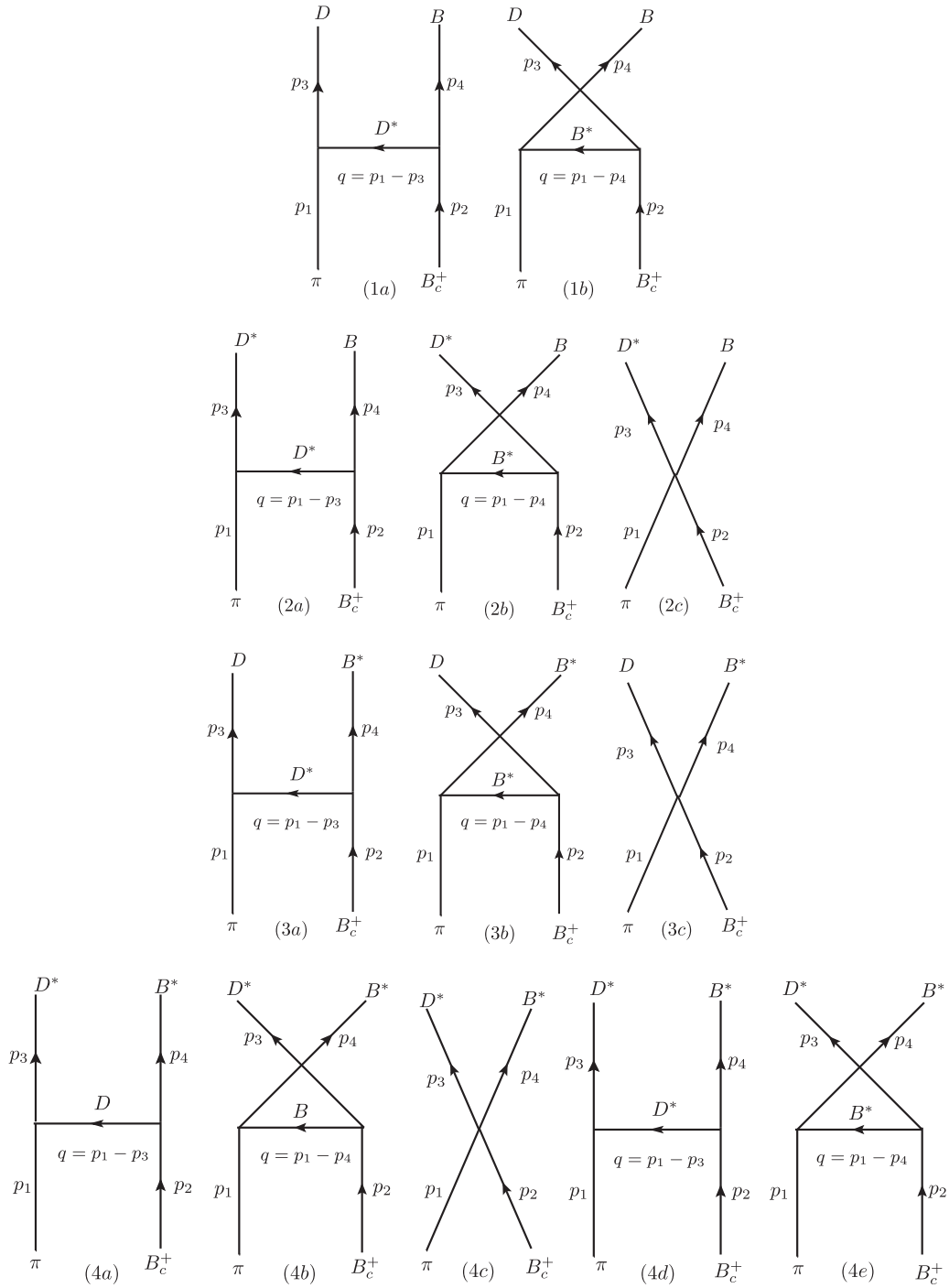


FIG. 1. Feynman diagrams of $B_c$ dissociation processes (1) $B_c^+ + \pi \to D + B$, (2) $B_c^+ + \pi \to D^* + B$, (3) $B_c^+ + \pi \to D + B^*$, and (4) $B_c^+ + \pi \to D^* + B^*$. All diagrams of the processes (2) and (3) and (4d), (4e) diagrams of the process (4) are produced by anomalous couplings.

and the full amplitude is given by

$$M_5 = M_{5a} + M_{5b} + M_{5c}. \tag{12d}$$

Diagrams of the process $B_c^+ + \rho \to D^* + B$ are shown in Fig. 2 (6a to 6d). The amplitude of the anomalous diagram 6d is given as

$$M_{6d} = g_{\rho B^* B} g_{B_c B^* D^*} \varepsilon_{\delta\gamma\sigma\lambda} \varepsilon_{\alpha\beta}^{\delta\gamma} p_1^{\sigma} p_4^{\lambda} (p_3 - p_1)_{\mu} \frac{-i}{t - m_{B^*}^2} \left( g^{\alpha\beta} - \frac{(p_1 - p_3)^{\alpha} (p_1 - p_3)^{\beta}}{m_{B^*}^2} \right) (p_4 - p_2)_{\nu} \varepsilon_{\rho}^{\mu}(p_1) \varepsilon_{D^*}^{\nu}(p_4), \tag{13a}$$

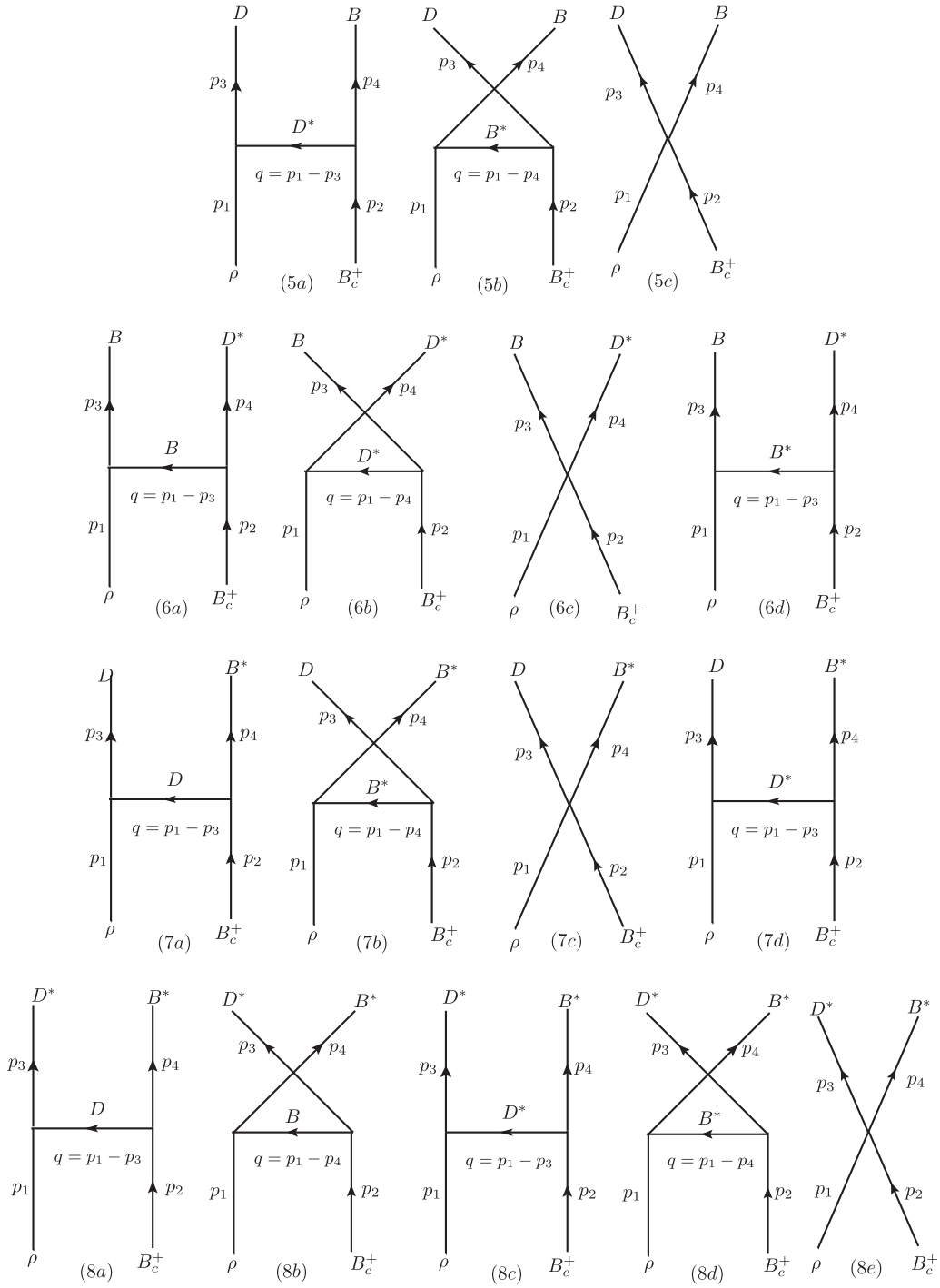


FIG. 2. Feynman diagrams of $B_c$ dissociation processes (5) $B_c^+ + \rho \to D + B$, (6) $B_c^+ + \rho \to D^* + B$, (7) $B_c^+ + \rho \to D + B^*$, and (8) $B_c^+ + \rho \to D^* + B^*$. All diagrams of the processes (5) and (8) and (6d), (7d) diagrams of the processes (6) and (7), respectively, are produced by the anomalous couplings.

and the full amplitude is written as

$$M_6 = M_{6a} + M_{6b} + M_{6c} + M_{6d}. \tag{13b}$$

Diagrams of the process $B_c^+ + \rho \to D + B^*$ are shown in Fig. 2 (7a to 7d). The amplitude of the anomalous diagram 7d is given as

$$M_{7d} = g_{\rho D^* D} g_{B_c B^* D^*} \varepsilon_{\sigma\lambda\gamma\delta} \varepsilon_{\alpha\beta}^{\gamma\delta} p_1^\sigma p_4^\lambda (p_3 - p_1)_\mu \frac{-i}{t - m_{D^*}^2} \left( g^{\alpha\beta} - \frac{(p_1 - p_3)^\alpha (p_1 - p_3)^\beta}{m_{D^*}^2} \right) (p_2 - p_4)_\nu \, \varepsilon_\rho^\mu(p_1) \varepsilon_{D^*}^\nu(p_4). \tag{14a}$$

And the full amplitude is written as

$$M_7 = M_{7a} + M_{7b} + M_{7c} + M_{7d}. \tag{14b}$$

Diagrams of the process $B_c^+ \rho \to D^* + B^*$ are shown in Fig. 2 (8a to 8e) and corresponding amplitudes are

$$M_{8a} = g_{\rho D^* D} g_{B_c B^* D} \boldsymbol{\varepsilon}_{\mu\nu\alpha\beta} p_1^\alpha (p_3 - p_1)^\beta \frac{i}{t - m_D^2} (p_4 - 2p_2)_\lambda \varepsilon_\rho^\mu(p_1) \varepsilon_{D^*}^\nu(p_3) \varepsilon_{B^*}^\lambda(p_4), \tag{15a}$$

$$M_{8b} = -g_{\rho BB^*} g_{B_c BD^*} \varepsilon_{\mu\lambda\alpha\beta} p_1^\alpha p_4^\beta \frac{i}{u - m_B^2} (p_3 - 2p_2)_\nu \varepsilon_\rho^\mu(p_1) \varepsilon_{D^*}^\nu(p_3) \varepsilon_{B^*}^\lambda(p_4), \tag{15b}$$

$$M_{8c} = g_{\rho D^* D^*} g_{B_c B^* D^*} \varepsilon_{\delta\alpha\beta}^\sigma p_4^\delta \frac{-i}{t - m_{D^*}^2} [(2p_3 - p_1)_\mu g_{\sigma\nu} + (2p_1 - p_3)_\nu g_{\mu\sigma} + (-p_3 - p_1)_\sigma g_{\mu\nu}]$$
$$\times \left( g^{\alpha\beta} \frac{(p_1 - p_3)^\alpha (p_1 - p_3)^\beta}{m_{D^*}^2} \right) (p_4 - p_2)_\lambda \varepsilon_\rho^\mu(p_1) \varepsilon_{D^*}^\nu(p_3) \varepsilon_{B^*}^\lambda(p_4), \tag{15c}$$

$$M_{8d} = g_{\rho B^* B^*} g_{B_c B^* D^*} \varepsilon_{\delta\alpha\beta}^\sigma p_3^\delta \frac{-i}{u - m_{B^*}^2} [(-2p_4 + p_1)_\lambda g_{\sigma\mu} + (p_1 + p_4)_\sigma g_{\mu\lambda} + (p_4 - 2p_1)_\mu g_{\sigma\lambda}]$$
$$\times \left( g^{\alpha\beta} - \frac{(p_1 - p_4)^\alpha (p_1 - p_4)^\beta}{m_{B^*}^2} \right) (p_2 - p_3)_\nu \times \varepsilon_\rho^\mu(p_1) \varepsilon_{D^*}^\nu(p_3) \varepsilon_{B^*}^\lambda(p_4), \tag{15d}$$

$$M_{8e} = \left( -i g_{\rho B_c B^* D^*} \varepsilon_{\mu\nu\lambda\beta} p_2^\beta + i h_{\rho B_c B^* D^*} \varepsilon_{\mu\nu\lambda\beta} p_4^\beta \right) \varepsilon_\rho^\mu(p_1) \varepsilon_{D^*}^\nu(p_3) \varepsilon_{B^*}^\lambda(p_4), \tag{15e}$$

and the full amplitude is written as

$$M_8 = M_{8a} + M_{8b} + M_{8c} + M_{8d} + M_{8e}. \tag{15f}$$

We define the four-momenta of the incoming particles by $p_1$ and $p_2$ and those of the final particles by $p_3$ and $p_4$, so that $t = (p_1 - p_3)^2$ and $s = (p_1 + p_2)^2$. Here $m_D$, $m_{D^*}$, $m_B$, and $m_{B^*}$ represent the masses of $D$, $D^*$, $B$, and $B^*$ mesons, respectively. The polarization vector of a vector meson with momentum $p_i$ is represented by $\varepsilon_i(p_i)$. After averaging (summing) over initial (final) spins and including isospin factor, we calculate isospin averaged cross sections by using the total amplitudes given in above equations. The isospin factor for calculating these cross sections is 2 for all the processes.

## III. $B_c$ MESON DISSOCIATION CROSS SECTIONS

### A. Numerical values of input parameters

Numerical values of all the meson masses are taken from Particle Data Group [28]. Estimation of the coupling constants of the effective Lagrangian is required for calculating the cross sections. To fix the couplings for the normal processes, we follow the methods of Refs. [12,29]; we refer to Ref. [12] for details. In a similar way, we have determined the couplings for the anomalous interactions, which are reported in this paper, whereas normal couplings are given in Refs. [23,24]. The coupling $g_{D^* D^* \pi}$, which has dimension $\mathrm{GeV}^{-1}$, is fixed by applying the heavy quark spin symmetry. We follow Ref. [25] in which this coupling is given as

$$g_{D^* D^* \pi} = \frac{g_{D^* D\pi}}{\langle m_D \rangle} \approx 9.08\ \mathrm{GeV}^{-1}, \tag{16}$$

where $\langle m_D \rangle$ represents the average mass of $D$ and $D^*$.

For $g_{\rho D^* D}$ couplings, we can apply the vector meson dominance (VMD) model [12] to the radiative decay of $D^*$ into $D$, i.e., $D^* \to D\gamma$. We use the same method as in Ref. [25]; this gives

$$g_{\rho D^* D} = 2.82\ \mathrm{GeV}^{-1}. \tag{17}$$

The coupling constants $g_{\rho B^* B}$, $g_{B_c B^* D^*}$, $g_{\pi B^* B^*}$ can be approximated in heavy quark mass limit, as in Ref. [30], by $g_{\rho BB}/\langle m_B \rangle$, $g_{B_c B^* D}/\langle m_D \rangle$, and $g_{\pi B^* B}/\langle m_B \rangle$, respectively. Since no experimental or phenomenological information is available for the four-point vertices, we use SU(5) symmetry relations to relate four-point couplings to the product of two three-point couplings and assume that the symmetry breaking effects in the four-point coupling constants are included via phenomenological values of the three-point couplings, as argued in Ref. [12]. These symmetry relations are derived in Refs. [23,24]. Here we report them along with the values of two four-point couplings as follows:

$$g_{\rho B_c D^* B^*} = h_{\rho B_c D^* B^*} = 2 g_{\rho D^* D} g_{B_c B D^*} \approx 67\ \mathrm{GeV}^{-1}. \tag{18}$$

However, for $g_{\pi B_c B^* D}$, $g_{\pi B_c D^* B}$, and $g_{\rho B_c D B}$ couplings, it is not possible to write these couplings as a product of two three-point coupling constants because they carry different dimensions. Hence, in this case, we directly use SU(5) symmetry relation assuming the symmetry breaking effects change $F_\pi$ to $F_D$ as in Ref. [25], where $F_\pi$ and $F_D$ are pion and $D$ meson decay constants, respectively. Here we have used $F_D \approx 2.3 F_\pi$ as in Ref. [25]. This gives

$$g_{\pi B_c D B^*} = g_{\pi B_c D^* B} = g_{\rho B_c D B} = \frac{3 g_{B_c D B^*}}{6\pi^2 F_D^3} \approx 21.56\ \mathrm{GeV}^{-3}. \tag{19}$$

The three-point coupling $g_{B_c D B^*}$ is given in Refs. [23,24]. We summarize the values of the coupling constants and methods for obtaining them in Table I.

TABLE I. Coupling constants of anomalous interactions $B_c$ with $\pi$ and $\rho$ mesons.

| Coupling constant | Value | Method of derivation |
|---|---|---|
| $g_{\pi D^* D^*}$ | 9.08 GeV$^{-1}$ | Heavy quark symmetry |
| $g_{\pi B^* B^*}$ | 2.34 GeV$^{-1}$ | Heavy quark symmetry |
| $g_{B_c B^* D^*}$ | 6.134 GeV$^{-1}$ | Heavy quark symmetry |
| $g_{\pi B_c D^* B}$ | 21.56 GeV$^{-3}$ | SU(5) symmetry |
| $g_{\pi B_c D B^*}$ | 21.56 GeV$^{-3}$ | SU(5) symmetry |
| $g_{\rho D^* D}$ | 2.82 GeV$^{-1}$ | VMD |
| $g_{\rho B^* B}$ | 2.58 GeV$^{-1}$ | Heavy quark symmetry |
| $g_{\rho B_c B D}$ | 21.56 GeV$^{-3}$ | $SU(5)$ symmetry |
| $g_{\rho B_c D^* B^*}$ | 67 GeV$^{-1}$ | $SU(5)$ symmetry |

### B. $B_c$ dissociation cross sections

In the effective hadronic Lagrangian, the hadrons represent the fundamental degrees of freedom. This treatment needs to be corrected by the inclusion of form factors as the hadrons are not the fundamental particles and have finite sizes. The resulting change in the transition amplitude of any diagram can be accounted for by multiplying with the form factors of the interaction vertices involved in it. In this paper, we have used the same monopole form factor as given in Refs. [23,24,27] to be multiplied with three-point vertices of all the processes:

$$f_3 = \frac{\Lambda^2}{\Lambda^2 + \mathbf{q}^2}. \tag{20}$$

Here, $\Lambda$ represents a cutoff parameter and $\mathbf{q}^2 = (\mathbf{p}_1 - \mathbf{p}_3)^2_{\rm cm}$ for $t$-channel diagrams and $(\mathbf{p}_1 - \mathbf{p}_4)^2_{\rm cm}$ for $u$-channel diagrams. This form factor was also used to calculate the cross sections of $B_c^+$ by $\pi$, $\rho$ mesons and nucleons in Refs. [22–24,27] and also in Refs. [12,13,31] to calculate the hadronic cross sections of charmonium, bottomonium, and $\eta$ mesons. For four-point interaction vertices we use the following form factor:

$$f_4 = \left(\frac{\Lambda^2}{\Lambda^2 + \bar{\mathbf{q}}^2}\right)^2, \tag{21}$$

where $\bar{\mathbf{q}}^2 = \frac{1}{2}[(\mathbf{p}_1 - \mathbf{p}_3)^2 + (\mathbf{p}_1 - \mathbf{p}_4)^2]_{\rm cm}$. Generally, the cutoff parameter may take different values for different vertices. In some cases, cutoff parameters of the form factors used within meson or baryon exchange models can be fitted to experimental data of hadronic cross sections [32]. In the absence of any experimental data, we may provide an estimate on the basis of the size of the interacting hadrons. It is shown in Ref. [23] that a variation of the cutoff parameter in the range 1.2 to 1.8 GeV is consistent with the known sizes of the interacting hadrons. As in the previous studies [23–25] and also based on the results given in Ref. [33], we consider the same cutoff parameters for all the processes and use two values 1 and 2 GeV.

Figures 3(a)–3(d) show the cross sections for $B_c$ dissociation with (dashed curves) and without (solid curves) form factor for the processes (a) $B_c^+ + \pi \to D + B$, (b) $B_c^+ + \pi \to D^* + B$, (c) $B_c^+ + \pi \to D + B^*$, and (d) $B_c^+ + \pi \to D^* + B^*$ as a function of total cm energy $\sqrt{s}$. Lower and upper

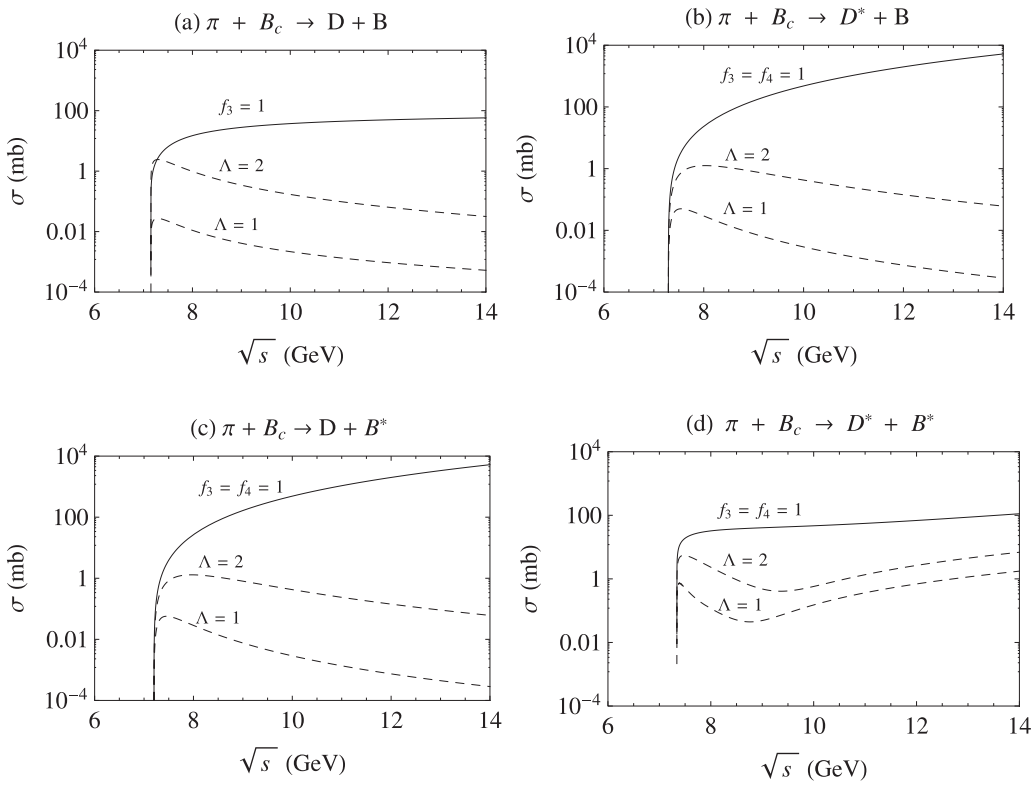


FIG. 3. Cross sections of $B_c$ dissociation processes (a) $B_c^+\pi \to DB$, (b) $B_c^+\pi \to D^*B$, (c) $B_c^+\pi \to DB^*$, and (d) $B_c^+\pi \to D^*B^*$ with (dashed curves) and without (solid curves) form factors.

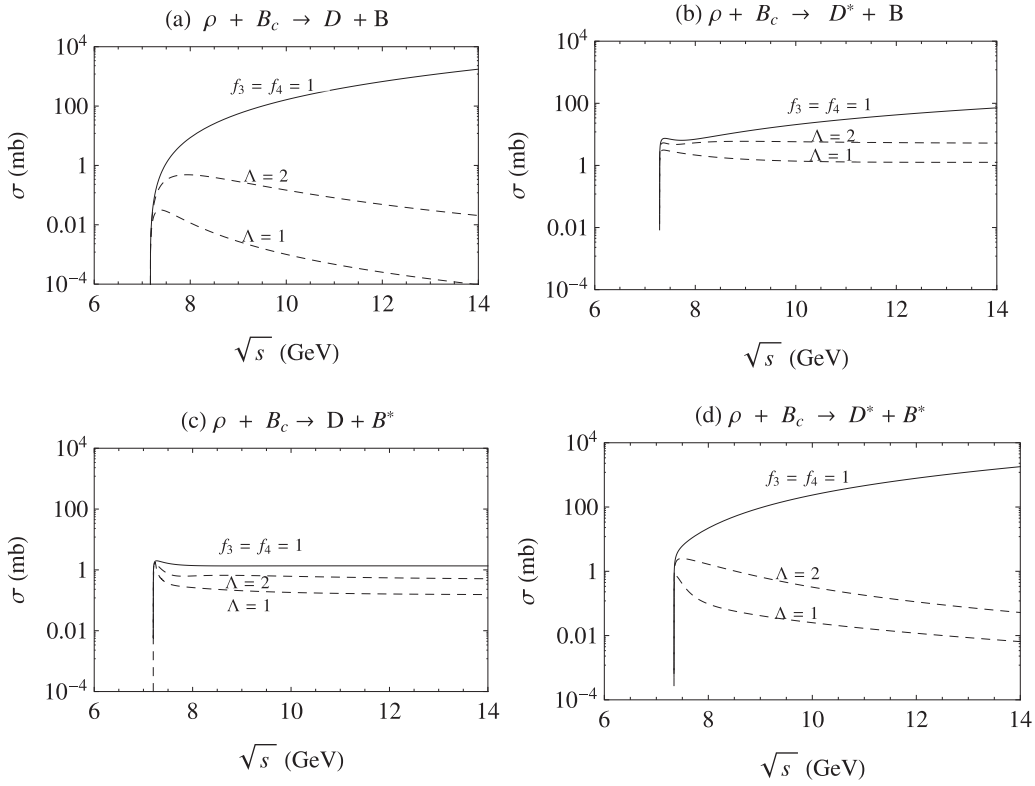


FIG. 4. Cross sections of $B_c$ dissociation processes (a) $B_c^+\rho \to DB$, (b) $B_c^+\rho \to D^*B$, (c) $B_c^+\rho \to DB^*$, and (d) $B_c^+\rho \to D^*B^*$ with (dashed curves) and without (solid curves) form factors.

dashed curves are with cutoff parameters $\Lambda = 1$ and 2 GeV, respectively. It can be seen that including the form factors substantially suppress the cross sections. However, the cross sections remain rapidly increasing at the threshold for all four processes, followed by a steady decrease. The process (a) is a normal process that does not include any anomalous diagram. The threshold energy of this process is 7.15 GeV. It can be seen from Fig. 3(a) that the cross section of this process varies from 0.02 to 2 mb near threshold depending on the value of $\Lambda$. The same plot is also reported in our previous work [23] without isospin averaging factor. For anomalous processes (b) and (c), the cross sections are almost the same, each varying from 0.05 to 1 mb near threshold depending on the values of $\Lambda$, as shown in Figs. 3(b) and 3(c). For the process (d), additional anomalous diagrams are included which are shown in Fig. 1 as diagrams (4d) and (4e). Figure 3(d) shows that the cross section of this process varies from 0.8 to 6 mb near threshold depending on the value of $\Lambda$. This cross section is also reported in our previous work [23] without including the anomalous diagrams.

Figures 4(a)–4(d) show the cross sections for $B_c$ dissociation with (dashed) and without (solid) form factor for the processes (a) $B_c^+ + \rho \to D + B$, (b) $B_c^+ + \rho \to D^* + B$, (c) $B_c^+ + \rho \to D + B^*$, and (d) $B_c^+ + \rho \to D^* + B^*$, respectively, as a function of the total cm energy $\sqrt{s}$. The cross sections with form factor are rapidly increasing at the threshold, followed by a steady decrease. For the processes (a) and (b) the cross sections vary in the range 0.2 to 0.4 mb and 2 to 3 mb, respectively, near threshold, whereas for (c) it almost remains 1.5 mb near threshold irrespective of the value of $\Lambda$. For the process (d), cross section varies in the range 0.8 to 1.2 mb near threshold depending on the value of $\Lambda$. It is noted that both (a) and (d) are anomalous processes, whereas for (b) and (c) additional diagrams are introduced by anomalous interactions. Previously in Ref. [24] we have studied (b) and (c) processes without including the anomalous diagrams.

### C. Thermal averaged cross sections

The following formula is used to calculate the thermal averaged cross sections [31]:

$$\langle \sigma \upsilon \rangle = \left[4\alpha_1^2 K_2(\alpha_1)\alpha_2^2 K_2(\alpha_2)\right]^{-1} \times \int_{z_0}^{\infty} dz[z^2 - (\alpha_1+\alpha_2)^2 \times [z^2 - (\alpha_1-\alpha_2)^2]K_1(z)\sigma(s = z^2T^2), \quad (22)$$

with $\alpha_i = m_i/T$, $z_0 = \max(\alpha_1+\alpha_2, \alpha_3+\alpha_4)$, $K_1$ and $K_2$ are the modified Bessel functions of second kind of order 1 and 2, respectively, $\upsilon$ is the relative velocity of initial particles, and $T$ is the temperature of the hadronic matter. We have calculated the thermal averaged cross sections of $B_c$ mesons with form factors as a function of temperature $T$. Figure 5 shows the temperature dependence of thermal averaged cross sections for all four processes of $B_c$ dissociation by $\pi$. The range of the temperature is taken from 0.1 to 0.3 GeV. To highlight the contribution of anomalous diagrams which contribute in the process (d) $B_c^+\pi \to D^*B^*$, we plot the cross sections in Fig. 5(d) with (solid curve) and without (dashed

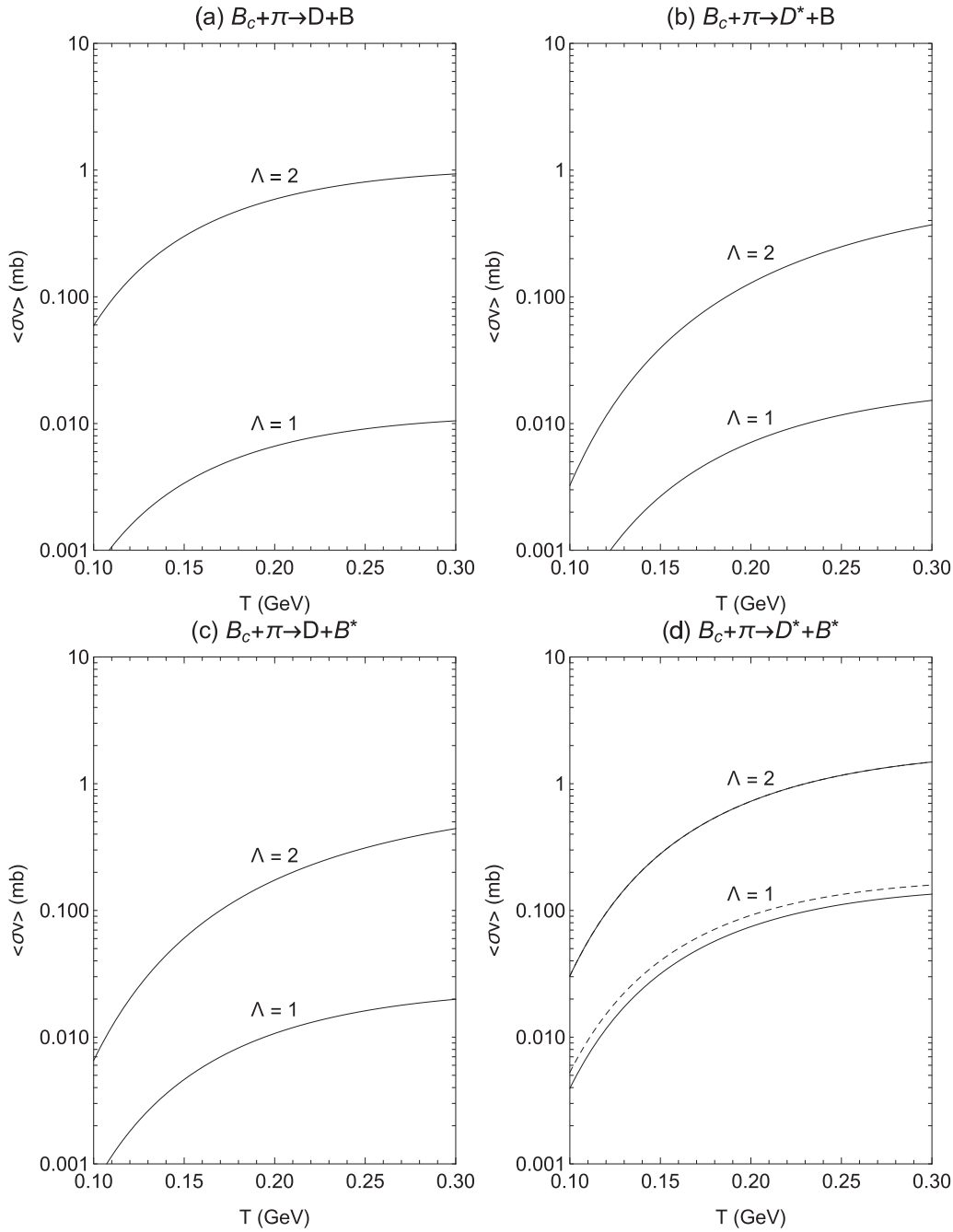


FIG. 5. Thermal averaged cross sections of $B_c$ dissociation processes (a) $B_c^+\pi \to DB$, (b) $B_c^+\pi \to D^*B$, (c) $B_c^+\pi \to DB^*$, and (d) $B_c^+\pi \to D^*B^*$ as a function of temperature. Solid and dashed curves represent cross sections with and without anomalous contribution, respectively.

curve) anomalous diagrams. For $\Lambda = 1$ GeV, the average decrease in cross section due to anomalous interactions is about 25%, whereas for $\Lambda = 2$ GeV it is less than 0.1%. In Fig. 6 thermal averaged cross sections with form factor, of $B_c$ meson dissociation by $\rho$ mesons are given. The figure shows that the contribution of the process (b) $B_c^+ + \rho \to D^* + B$ is highest. In Figs. 6(b) and 6(c) we highlight the contribution of anomalous diagrams by showing the plots of cross sections with (solid curves) and without (dashed curved) anomalous diagrams. Figure 6(b) shows that anomalous couplings substantially suppress the cross section of the process (b), whereas for the process (c) the change is relatively small as shown in Fig. 6(c). In Fig. 6(c), the average decrease in cross section due to anomalous couplings is about 40% for $\Lambda = 1$ GeV, whereas for $\Lambda = 2$ GeV, it is increased by 2%. It is also noted that in Fig. 6(b) anomalous couplings change the slop of the cross section curve for $\Lambda = 2$ GeV. Thermal averaged cross sections reported here are used to study yield of $B_c$ mesons in the hadronic matter in the next section.

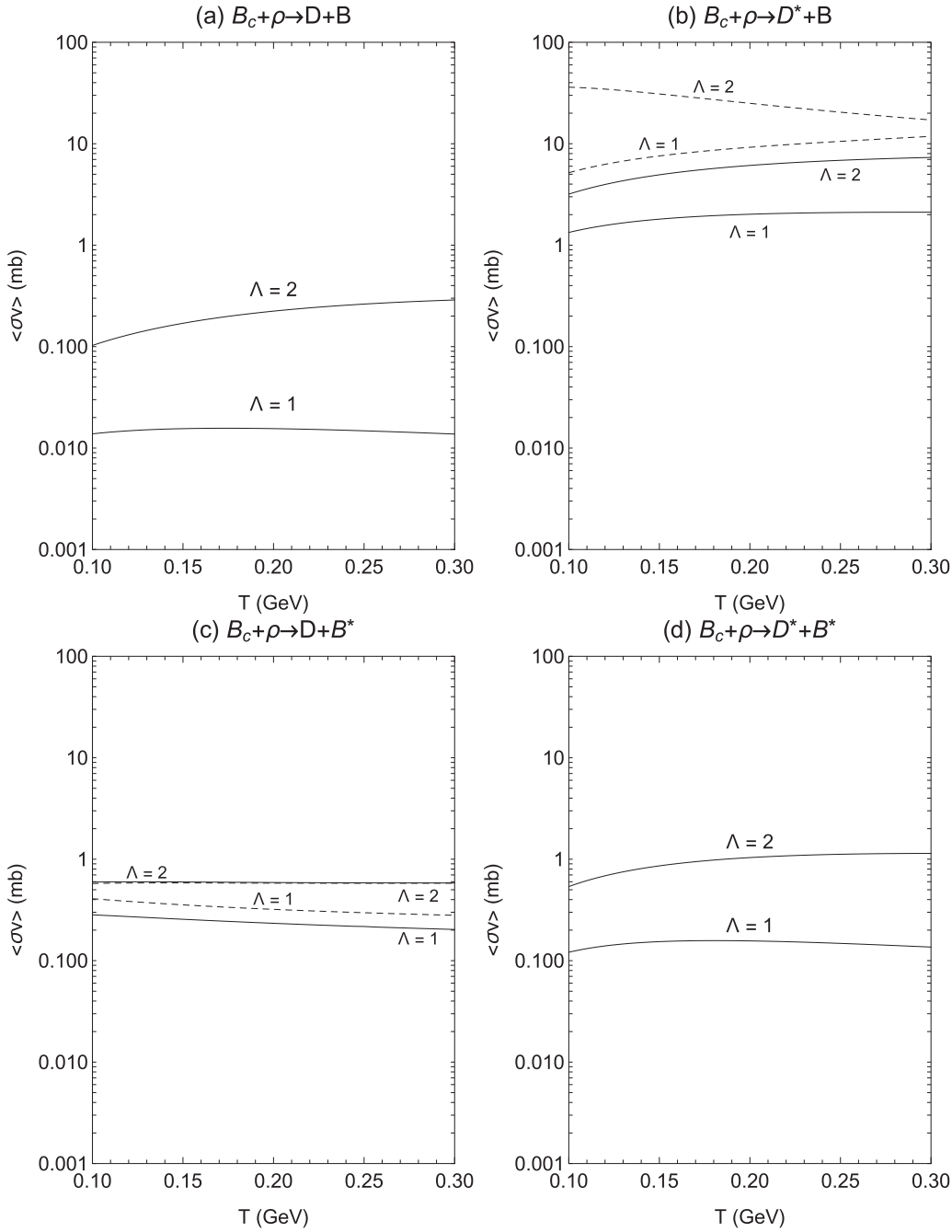


FIG. 6. Thermal averaged cross sections of $B_c$ dissociation processes (a) $B_c^+\rho \to DB$, (b) $B_c^+\rho \to D^*B$, (c) $B_c^+\rho \to DB^*$, and (d) $B_c^+\rho \to D^*B^*$ as a function of temperature. Solid and dashed curves represent cross sections with and without anomalous contribution, respectively.

## IV. DISSOCIATION RATE OF $B_c$ AT LHC

Now we examine the effect of interactions of $B_c$ meson with the comovers on its production rate in the hot hadronic matter. The time evolution of $B_c$ abundance is studied at LHC energy using a schematic expanding fireball model with initial abundance determined by the cross sections calculated using a complete pQCD approach.

### A. Time evolution of $B_c$ Mesons

Time evolution of $B_c$ meson density in the hot hadronic matter can be studied by the rate equation

$$\partial_\mu(n_{B_c}u^\mu) = \Psi, \tag{23}$$

where $\Psi$ is composed of the source (the processes in which $B_c$ mesons are created) and/or the sink (the processes in which

$B_c$ mesons are dissociated) terms, $u^\mu = \gamma(1, \mathbf{v})$ is the four velocity and is specified in terms of fluid velocity ($\mathbf{v}$) of the hadronic matter and Lorentz factor $\gamma$ [31], and $n_{B_c}$ is the density of $B_c$ mesons.

The source term in $\Psi$, represented by $\Psi_1$, is given as

$$\Psi_1 = \sum_{a,b,c} \langle \sigma_{bc\to B_c a} v_{bc} \rangle n_b n_c, \tag{24}$$

and the sink term in $\Psi$, represented by $\Psi_2$, is given by

$$\Psi_2 = \sum_{a,b,c} \langle \sigma_{B_c a\to bc} v_{B_c a} \rangle n_{B_c} n_a. \tag{25}$$

Here $a = \pi, \rho$; $b = B, B^*$; and $c = D, D^*$, and $n_a, n_{B_c}, n_b$, and $n_c$ represent the densities of $a, B_c, b$, and $c$ mesons, respectively. Thus, $\Psi$ can be expressed as

$$\Psi = \sum_{a,b,c} \langle \sigma_{bc\to B_c a} v_{bc} \rangle n_b n_c - \sum_{a,b,c} \langle \sigma_{B_c a\to bc} v_{B_c a} \rangle n_{B_c} n_a, \tag{26}$$

where $\langle \sigma_{aB_c\to bc} v_{B_c a} \rangle$ and $\langle \sigma_{bc\to B_c a} v_{bc} \rangle$ represent thermal averaged cross sections of $B_c$ dissociation with the comoving particle $a$ and production of $B_c$ through corresponding reverse process, respectively. We assume for the sake of simplicity that the comovers almost remain in chemical equilibrium throughout the course of their interaction with $B_c$ mesons, so that the densities of $a$, $b$, and $c$ particles (except $B_c$) are assumed to take their equilibrium values:

$$n_{a,b,c} \approx n^{\rm eq}_{a,b,c}. \tag{27}$$

In chemical equilibrium, the principle of detailed balance holds and hence the production rate of $B_c$ mesons is equal to its rate of dissociation:

$$\langle \sigma_{B_c a\to bc} v_{B_c a} \rangle n^{\rm eq}_{B_c} n^{\rm eq}_a = \langle \sigma_{bc\to B_c a} v_{bc} \rangle n^{\rm eq}_b n^{\rm eq}_c, \tag{28}$$

The equilibrium density $n^{\rm eq}$ [34] of a hadron is given as

$$n^{\rm eq} = \frac{dm^2 T}{2\pi^2} K_2(m/T), \tag{29}$$

where $K_2$ is the modified Bessel function of the second kind and second order, $m$ is the mass of the hadron, and $d = (2S + 1)(2I + 1)$ is its degeneracy factor due to spin $S$ and isospin $I$. Using Eqs. (24)–(28) in Eq. (23), we get

$$\partial_\mu (n_{B_c} u^\mu) = \sum_{a,b,c} \langle \sigma_{B_c a\to bc} v_{B_c a} \rangle \left( n^{\rm eq}_{B_c} - n_{B_c} \right) n^{\rm eq}_a. \tag{30}$$

To determine the time evolution of the transverse radius of the fireball, we use the hydrodynamic model as in Ref. [31]. In LHC the particles are distributed almost uniformly in the central rapidity region. We use cylindrical coordinates $(\tau, \eta, r, \phi)$ due to cylindrically symmetric geometry of collision. Here $\tau$, $\eta$, $r$, and $\phi$ represent longitudinal proper time, space-time rapidity, transverse radius, and polar angle, respectively. The proper time $\tau$ and rapidity are defined as

$$\tau = (t^2 - z^2)^{\frac{1}{2}}, \quad \eta = \frac{1}{2} \ln \frac{t+z}{t-z}. \tag{31}$$

The density $n_{B_c}(\tau, \eta, r, \phi)$ remains constant in $\phi - r$ plane due to cylindrical symmetry. The assumption of radial transverse expansion implies that $u^\phi = u^\eta = 0$ [31]. Further assuming that in the transverse plane density is uniform. Applying these assumptions and averaging over the radial coordinate [35,36], we get

$$\frac{1}{\tau R^2(\tau)} \frac{\partial}{\partial \tau} [\tau R^2(\tau) n_{B_c} \langle u^\tau \rangle] = \sum_{a;b;c} \langle \sigma_{B_c a\to bc} v_{B_c a} \rangle (n^{\rm eq}_{B_c} - n_{B_c}) n^{\rm eq}_a. \tag{32}$$

Here $R(\tau)$ is the transverse radius of the fireball [31], and $\langle u^\tau \rangle$ represents the averaged $\tau$ component of four-velocity vector which is expressed as

$$\langle u^\tau \rangle = \frac{2}{R^2(\tau)} \int_0^{R(\tau)} dr r u^\tau(r). \tag{33}$$

The expression of $u^\tau$ in terms of $\beta_r$ (radial flow velocity of the hadronic matter) can be written as

$$u^\tau(t) = \frac{1}{\sqrt{1 - \beta_r^2}}, \tag{34}$$

where $\beta_r$ is taken

$$\beta_r(\tau, r) = \frac{dR}{d\tau} \left( \frac{r}{R} \right)^a. \tag{35}$$

Here $a$ is a constant and its value is taken to be 1 as in Refs. [31,34]. $\langle u^\tau \rangle$ of Eq. (33) can now be written as

$$\langle u^\tau(t) \rangle = \int_0^1 dy \frac{1}{\sqrt{1 - (dR/d\tau)^2 y}}. \tag{36}$$

We use the following ansatz to describe the time evolution of the transverse radius of the fireball:

$$R(\tau) = R_H + v_H(\tau - \tau_H) + \frac{a_H}{2}(\tau - \tau_H)^2, \tag{37}$$

where $R_H$ and $v_H$ represent transverse radius and transverse flow velocity of fireball, respectively, at hadronization, while $a_H = 0.02$ fm$^{-1}$, taken from Ref. [31], is the traverse acceleration of expansion. This implies that $\langle u^\tau \rangle$ is given by

$$\langle u^\tau(t) \rangle = \frac{2}{1 + \sqrt{1 - (a_H(\tau - \tau_H) + v_H)^2}}. \tag{38}$$

To solve the evolution Eq. (32), we require time variation of temperature, which can be obtained by applying the condition of entropy conservation as follows:

$$\tau R^2(\tau) \langle u^\tau(t) \rangle s(T) = \tau_0 R^2(\tau_0) \langle u^\tau(t_0) \rangle s(T_0), \tag{39}$$

where $s(T)$ is the entropy density which is given by

$$s(T) = \sum_i \frac{d_i}{2\pi^2} m_i^3 K_3(m_i/T), \tag{40}$$

with $i = \pi$, $K$, $\rho$, $\omega$, $K^*$ and $d_i$ is the degeneracy factor. We take hadronization temperature $T_H = 0.17$ GeV. The freeze-out temperature $T_F \approx 0.1$ GeV and averaged transverse flow velocity $\simeq 0.65$ at kinetic freeze-out are obtained from the fit of low $p_T$ spectra of light hadrons at $\sqrt{s_{\rm NN}} = 2.76$ with hydrodynamics-inspired blast-wave models in Ref. [37]. We use the extracted value of the fireball volume $\sim$5000 fm$^3$ [38] at freeze-out in Pb+Pb collisions at $\sqrt{s_{\rm NN}} = 2.76$ TeV for 5% most central events. The freeze-out time $\tau_F = 10$ fm/c is

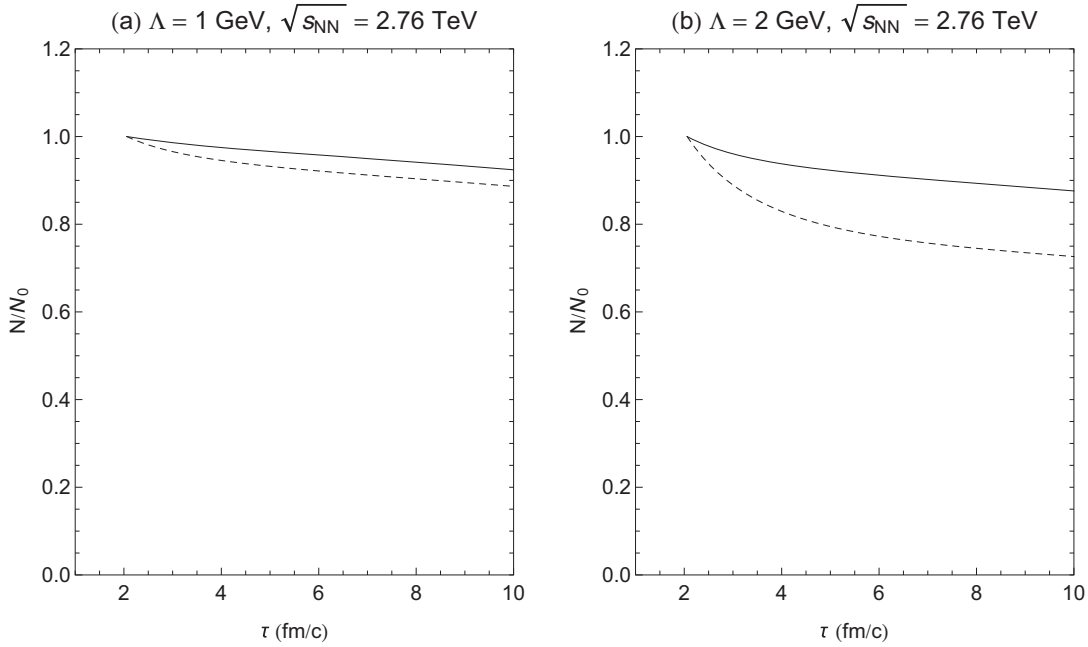


FIG. 7. Time evolution of $B_c$ meson abundance (normalized to initial value) at $\sqrt{s_{NN}} = 2.76$ TeV, with (solid curves) and without anomalous (dashed curves) contributions, from hadronization time $\tau_H = 2$ fm/c to freeze-out time $\tau_F = 10$ fm/c. For the left panel cutoff parameter $\Lambda = 1$ GeV and for the right panel $\Lambda = 2$ GeV.

obtained from the study of two-pion Bose-Einstein correlations in LHC at $\sqrt{s_{NN}} = 2.76$ [39]. All these values are used in Eqs. (37)–(40) to find fitted values of $R_H \approx 8$ fm, $\tau_H \approx 2$ fm/c, and $v_H \approx 0.5$. At present the measurements of fireball parameters are not available at $\sqrt{s_{NN}} = 5.05$ TeV. So we use the extrapolated values; 0.68 for transverse flow velocity and 5800 fm$^3$ for fireball volume at kinetic freeze-out temperature $T_F = 0.1$ GeV and time $\tau_F = 11$ fm/c using the results given in Ref. [40]. A fit of these values produces $\tau_H \approx 2.5$, whereas $R_H$ and $v_H$ virtually remain the same.

Finally, we require the abundance of $B_c$ meson at hadronization time to solve the rate Eq. (32). Since the temperature of the fireball is small as compared to masses of $c\bar{c}$ and $b\bar{b}$, therefore, it is unlikely that $B_c$ is produced at thermal stage of the process. We assume that all heavy flavor quark pairs are produced at the initial stage through hard parton collisions and their numbers remain approximately unchanged during time evolution of the fireball. Thus, averaged hard scattering yield of $B_c$ mesons at given centrality class is estimated by the following formula:

$$N_{B_c} = \frac{\sigma_{pp\to B_c}}{\sigma_{pp}^{(\mathrm{inel})}} N_{\mathrm{coll}} R_{\mathrm{cut}}, \tag{41}$$

where total inelastic cross section in pp collision $\sigma_{pp}^{(\mathrm{inel})} \approx 60$ and 72 mb for LHC at $\sqrt{s_{NN}} = 2.76$ and 5.05 TeV, respectively, $N_{\mathrm{coll}} = 1876$ is the number of primordial pp collisions for 5% most centered events, estimated using Glauber model [41]. The inclusive $B_c$ production cross section $\sigma_{pp\to B_c}$ is taken to be 53 and 97 nb at $\sqrt{s_{NN}} = 2.76$ and 5.05 TeV, respectively. These values include the contribution of $1^3S_1$, $2S$, and $1P$ $B_c$ states that are below $BD$ threshold, and hence cascade to $B_c$ ground state with 100% BR. The value at $\sqrt{s_{NN}} = 5.05$ TeV is calculated in Ref. [42] using complete pQCD approach. The details of these calculations and comparison to other methods are given in Ref. [43]. However, the Ref. [42] reports the cross sections for $1^1S_0$ and $1^3S_1$ states only. The production cross sections of $2^1S_0$ and $2^3S_1$ states are obtained by multiplying the corresponding values of $1S$ states with the factor $|R_{2S}(0)/R_{1S}(0)|^2 \simeq 0.6$ [44], whereas the cross section of $1P$ states is taken 50% of $B_c$ ground state as found in Ref. [45] using pQCD approach. The value at $\sqrt{s_{NN}} = 2.76$ TeV is obtained by extrapolation of logarithmic fit of the values at $\sqrt{s_{NN}} = 5.05$, 8.12, and 13 TeV given in Ref. [42]. The factor $R_{\mathrm{cut}}$ represents the fraction of $B_c$ mesons produced within given rapidity $y$ and $p_T$ cut. We take $R_{\mathrm{cut}} = 0.48$ for $|y| < 2$ and $p_T > 5$ GeV [42]. With these inputs we find that $N_{B_c} \approx 7.9 \times 10^{-4}$ and $1.2 \times 10^{-3}$ at $\sqrt{s_{NN}} = 2.76$ and 5.05 TeV, respectively, for 0 to 5% centrality class.

By using thermal averaged cross sections given in the previous section and solving Eq. (32) numerically with initial abundance $N_0 = N_{B_c}$, the time dependence of $B_c$ meson yield in hadronic matter at LHC is calculated for $\Lambda = 1$ and 2 GeV. The resultant time-dependent yield for $\sqrt{s_{NN}} = 2.76$ TeV normalized to initial value (at $\tau = \tau_H$) is plotted in Fig. 7 using cross sections with (solid curves) and without (dashed curves) anomalous interaction. We take $\Lambda = 1$ and 2 GeV for Figs. 7(a) and 7(b), respectively. Figure 7 shows that the normalized yield of $B_c$ mesons slowly decreases with time in the hadronic matter. Total decrease with anomalous contribution is 8% and 12.5% for $\Lambda = 1$ and 2 GeV, respectively, and without anomalous contribution it is 11.5% and 27.5%, respectively, for $\sqrt{s_{NN}} = 2.76$ TeV. So the anomalous contribution significantly decreases the suppression of $B_c$ meson due to the comover effect for $\Lambda = 2$ GeV. In Fig. 8 we show the plots of time variation of normalized yield at $\sqrt{s_{NN}} =$

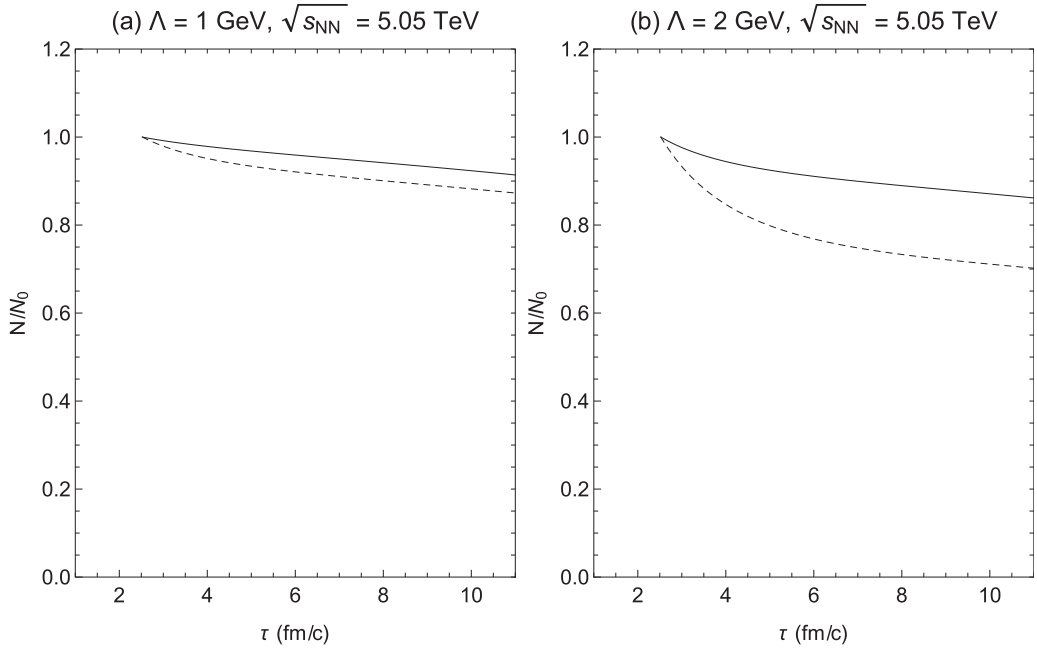


FIG. 8. Same as decribed in the caption of Fig. 7, except $\sqrt{s_{NN}} = 5.05$ TeV, hadronization time $\tau_H = 2.5$ fm/c, and freeze-out time $\tau_F = 11$ fm/c.

5.05 TeV. Total decrease with anomalous contribution is 9% and 14% for $\Lambda = 1$ and 2 GeV, respectively, and without anomalous contribution, it is 13% and 30%, respectively. So we find that normalized $B_c$ yield is somewhat more suppressed at higher value of center of mass energy in Pb-Pb collisions.

## V. CONCLUDING REMARKS

A knowledge of $B_c$ dissociation cross sections by the comovers (in this paper by $\pi$ and $\rho$ mesons) is essential to extract information on properties of QGP at LHC. In this paper, we have calculated cross sections for $B_c$ meson dissociation by $\pi$ and $\rho$ mesons using the meson exchange model including anomalous couplings like PVV, PPPV, and VVVP. Previously, we have studied these processes without including these couplings. We find that anomalous couplings significantly reduce the cross section of the dominant process $B_c^+ + \rho \to D^* + B$ both for $\Lambda = 1$ and 2 GeV as shown in Fig. 6. To study the effect of $B_c$ meson interactions with comovers in hot hadronic gas, we solve the kinetic equation for the heavy-ion collision dynamics at LHC. The plots show that the total suppression caused by the interactions of $B_c$ mesons with comovers is about 10%. This result shows that although the effect of interaction with comovers is small but it is not negligible. We also find that normalize yield of $B_c$ meson is not much affected by the value of the center of mass energy in Pb-Pb collisions.

## ACKNOWLEDGMENT

F.A. acknowledges the financial support of HEC of Pakistan through Project No. 20-4500/NRPU/R&D/HEC/14/727.

[1] T. Matsui and H. Satz, Phys. Lett. B **178**, 416 (1986).
[2] M. C. Abreu *et al.* NA50 Collaboration, Phys. Lett. B **450**, 456 (1999).
[3] W. Cassing and C. M. Ko, Phys. Lett. B **396**, 39 (1996); W. Cassing and E. L. Bratkovskaya, Nucl. Phys. A **623**, 570 (1997).
[4] N. Armesto and A. Capella, Phys. Lett. B **430**, 23 (1998).
[5] D. E. Kahana and S. H. Kahana, Phys. Rev. C **59**, 1651 (1999).
[6] C. Gale, S. Jeon, and J. Kapusta, Phys. Lett. B **459**, 455 (1999).
[7] C. Spieles, R. Vogt, L. Gerland, S. A. Bass, M. Bleicher, H. Stocker, and W. Greiner, Phys. Rev. C **60**, 054901 (1999).
[8] B.-H. Sa, A. Tai, H. Wang, and G.-H. Liu, Phys. Rev. C **59**, 2728 (1999).
[9] D. Kharzeev and H. Satz, Phys. Lett. B **334**, 155 (1994).
[10] D. Kharzeev, H. Satz, A. Syamtomov, and G. Zinovjev, Phys. Lett. B **389**, 595 (1996).
[11] C. Y. Wong, E. S. Swanson, and T. Barnes, Phys. Rev. C **62**, 045201 (2000); M. A. Ivanov, J. G. Korner, and P. Santorelli, Phys. Rev. D **70**, 014005 (2004).
[12] Z. Lin and C. M. Ko, Phys. Rev. C **62**, 034903 (2000).
[13] Z. Lin and C. M. Ko, Phys. Lett. B **503**, 104 (2001).
[14] K. L. Haglin, Phys. Rev. C **61**, 031902(R) (2000).
[15] W. Liu, C. M. Ko, and Z. W. Lin, Phys. Rev. C **65**, 015203 (2001).
[16] The annual Quark Matter conference 2011, reported in CERN Bulletin Nos. 21-22 (2011).
[17] R. Vogt, Phys. Rept. **310**, 197 (1997).

[18] M. Schroedter, R. L. Thews, and J. Rafelski, Phys. Rev. C **62**, 024905 (2000).
[19] J. Letessier and J. Refelski, *Hadrons and Quark-Gluon Plasma* (Cambridge University Press, Cambridge, UK, 2002).
[20] W. M. Alberico, S. Carignano, P. Czerski, A. De Pace, M. Nardi, and C. Ratti, Cent. Eur. J. Phys. **12**, 780 (2014).
[21] Yunpeng Liu, Carsten Greiner, and Andriy Kostyuk, Phys. Rev. C **87**, 014910 (2013).
[22] M. A. K. Lodhi and R. Marshall, Nucl. Phys. A **790**, 323 (2007).
[23] M. A. K. Lodhi, F. Akram, and S. Irfan, Phys. Rev. C **84**, 034901 (2011).
[24] Faisal Akram and M. A. K. Lodhi, Phys. Rev. C **84**, 064912 (2011).
[25] Yongseok, Taesoo Song, and Su Houng Lee, Phys. Rev. C **63**, 034901 (2001).
[26] R. S. Azevedo and M. Nielsen, Braz. J. Phys. **34**, 272 (2004).
[27] Faisal Akram and M. A. K. Lodhi, Nucl. Phys. A **877**, 95 (2012).
[28] M. Tanabashi *et al.* (Particle Data Group), Phys. Rev. D **98**, 030001 (2018).
[29] K. L. Haglin and C. Gale, Phys. Rev. C **63**, 065201 (2001).
[30] L.-H. Chan, Phys. Rev. D **55**, 5362 (1997).
[31] W. Liu a, C. M. Ko, and L. W. Chen, Nucl. Phys. A **765**, 401 (2006).
[32] R. Machleid, K. Holinde, and C. Elster, Phys. Rev. **149**, 1 (1987); R. Machleid, Adv. Nucl. Phys. **19**, 189 (1989); D. Lohse, J. W. Durso, K. Holinde, and J. Speth, Nucl. Phys. A **516**, 513 (1990).
[33] S. Yasui and K. Sudoh, Phys. Rev. D **80**, 034008 (2009).
[34] L. Alvarez-Ruso and V. Koch, Phys. Rev. C **65**, 054901 (2002).
[35] T. Biro, H. W. Barz, B. Lukacs, and J. Zimanyi, Phys. Rev. C **27**, 2695 (1983).
[36] C. M. Ko and L.-H. Xia, Phys. Rev. C **38**, 179 (1988).
[37] P. Foka and M. A. Janik, Rev. Phys. **1**, 154 (2016).
[38] J. Adam *et al.* (ALICE Collaboration), Phys. Rev. C **93**, 024905 (2016).
[39] K. Aamodt *et al.* (ALICE Collaboration), Phys. Lett. B **696**, 328 (2011).
[40] Anton Andronic, Int. J. Mod. Phys. A **29**, 1430047 (2014).
[41] David G. d'Enterria, arXiv:nucl-ex/0302016.
[42] C.-H. Chang and X.-G. Wu, Eur. Phys. J. C **38**, 267 (2004); G. Chen, C.-H. Chang, and X.-G. Wu, Phys. Rev. D **97**, 114022 (2018).
[43] N. Brambilla *et al.*, Eur. Phys. J. C **38**, 1534 (2011).
[44] K. Cheung and T. C. Yuan, Phy. Lett. B **325**, 481 (1994); Phys. Rev. D **53**, 1232 (1996).
[45] C.-H. Chang, J.-X. Wang, and X.-G. Wu, Phys. Rev. D **70**, 114019 (2004).